



## A multiple-band perfect absorber for SEIRA applications

Habibe Durmaz<sup>a,b,c,\*</sup>, Yuyu Li<sup>c</sup>, Arif E. Cetin<sup>d,\*</sup>

<sup>a</sup> Department of Electrical and Electronics Engineering, Karamanoglu Mehmetbey University, Yunus Emre Yerleşkesi, Karaman 70100, Turkey

<sup>b</sup> Department of Electrical and Electronics Engineering, Recep Tayyip Erdoğan University, Zihni Derin Yerleşkesi, Rize 53100, Turkey

<sup>c</sup> Department of Electrical and Computer Engineering and Photonics Center, Boston University, 8 Saint Mary's Street, Boston, MA, 02215, USA

<sup>d</sup> Izmir Biomedicine and Genome Center, 35340 Balcova, Izmir, Turkey

### ARTICLE INFO

#### Keywords:

Plasmonics  
Perfect absorber  
SEIRA  
Nano-fabrication

### ABSTRACT

Recently perfect absorbers (PAs) have received significant interest due to their characteristics of complex electric permittivity ( $\epsilon$ ) and magnetic permeability ( $\mu$ ). By rationally designing these artificial structures, the impedance of the perfect absorber can be matched to free space with an independent adjustment in the electric and magnetic resonances, where this structure leads to strong absorption from mid- to near-IR wavelength. In this article, we proposed a multiband PA platform, which simultaneously operates with a near unity absorption at different resonances that could be an ideal candidate for multiple sensing of molecular fingerprints. We numerically analyzed the dependence of the optical response of the PA platform through finite-difference time domain (FDTD) simulations for a fine-tuning mechanism of the PA platform. We theoretically demonstrated the surface enhanced infrared absorption (SEIRA) capability of our PA platform by studying its optical response with a thin protein bilayer and a polymethyl-methacrylate (PMMA) film. As an initial step we experimentally showed the vibrational modes of a thin PMMA film. We believe, our findings could open new avenues for reliable SERIA platforms through providing multiple vibrational finger print information compared to its conventional counterparts relying only on a single sensing data.

### 1. Introduction

Metamaterials have received significant attentions in many potential applications such as negative refraction [1–3], superlens [4], terahertz artificial dielectric cuboid lens on substrate for super-resolution images [5], and optical cloaking [6–8] due to its exotic electromagnetic nature. With the ability of adjustment in electric and magnetic resonances independently, it is possible to achieve impedance matching in free-space (i.e.  $z = \sqrt{\mu/\epsilon} = 1$ ) while minimizing the reflectance to zero. By using a lossy material and with the help of appropriate structural design of metamaterial, the various kinds of perfect absorbers have been designed for applications at different wavelength ranges from mid- to near-IR, such as photovoltaic cells [9], photodetectors [10], thermal emitters [11], plasmonic sensors [12], filters [13], and imagers [14,15]. Landy et al. [16] demonstrated the first PA with highly absorptive characteristics, tunable resonant frequency, and high Q-factor. Later, there have been many research reporting metamaterials based on PAs for single band [17], double band [18], wide band [19], and multiband [20] at different spectral ranges from microwave [21–24] to optical frequencies [25], including terahertz range [26].

Plasmonic resonances strongly depend on the surrounding dielectric medium at certain frequencies. Therefore, perfect absorbers have been utilized in highly sensitive spectroscopy applications, i.e., surface-enhanced infrared absorption spectroscopy (SEIRA) [27–31] and surface-enhanced Raman spectroscopy (SERS) [32–34]. Particularly, in SEIRA nano-antennas concentrate light on the antenna surface where the target molecules on the surface are interact effectively with the light in plasmon forms such that information of light-matter interaction with low analyte quantity can be easily identified. In SEIRA, nano-antennas are designed such that their operational frequency overlaps with the frequency of the vibrational modes of the target materials. The major drawback of this platform is that the sensing information is only based on a single vibration signature. This might cause reliability issues, which demands a sensing data associated with multiple vibrational signature of the targeted molecules. Therefore, there is a strong need for a sensing platform simultaneously monitor multiple vibrational modes of the molecules of interest. In this study, we proposed a SEIRA system that can be utilized to simultaneously identify multiple fingerprints of biomolecules. Compared to the current single mode SEIRA systems, our proposed platform will provide more reliable bio- and chemical sensing

\* Corresponding authors at: Habibe Durmaz, Department of Electrical and Electronics Engineering, Karamanoglu Mehmetbey University, Yunus Emre Yerleşkesi, Karaman 70100, Turkey; Izmir Biomedicine and Genome Center, 35340 Balcova, Izmir, Turkey.

E-mail addresses: [hdurmaz@kmu.edu.tr](mailto:hdurmaz@kmu.edu.tr) (H. Durmaz), [arif.engin.cetin@gmail.com](mailto:arif.engin.cetin@gmail.com) (A.E. Cetin).

<https://doi.org/10.1016/j.snb.2018.08.053>

Received 18 April 2018; Received in revised form 2 August 2018; Accepted 6 August 2018

Available online 09 August 2018

0925-4005/ © 2018 Elsevier B.V. All rights reserved.

information through simultaneous detection of multiple molecular vibrational modes. This will be achieved by exciting multiple antenna modes with different operating frequencies overlapping with different vibrational modes of the target molecules.

In general, the design of PAs can be divided into two categories based on their principle of operations. For the first category of absorbers, the operation of the devices rely on matching metamaterial impedance to free space, while simultaneously showing large effective permittivity and permeability in conductor. If the impedance matching is small i.e., large loss in conductor, then the surface will be reflectionless at normal incidence and incident field will attenuate rapidly within the conductor to a thin surface layer of few tens of nanometers once it is in contact with the surface. The second category of absorbers is based on electrically responsive metamaterial elements closely coupled to a ground plane. Typically, these absorbers consist of a resonant structure and have a narrow frequency response. These absorbers have the ability to absorb TM polarization nearly perfectly over all angles of incidence.

We introduced a composite PA system (which fits the first category) composed of U-shape antenna and a rectangular nano-bar (U-bar) shown in Fig. 1a [35]. The unit cell of the proposed system consists of three layers: gold layer at the bottom, resonators at the top and a magnesium fluoride ( $\text{SiO}_2$ ) layer between these metallic layers. The thickness of the bottom gold plane is chosen such that the transmission of the incident light through  $\text{SiO}_2$  layer is eliminated and to trap the light in  $\text{SiO}_2$  spacer through nearfield couplings between top Au bars and bottom Au film. In our composite PA system  $L$  is the length of the top rod,  $H$  is the length,  $K$  is the width of the bottom of the U-antenna,  $b$  is the width of the U-antenna, and  $a$  is the width of the top bar. The thicknesses of the U-bar antennas,  $\text{SiO}_2$  layer and bottom gold plane are 40, 140 and 200 nm, respectively. Fig. 1b shows finite-difference time-domain (FDTD) simulations (Lumerical Inc. FDTD Solutions). In the simulations, the mesh size is chosen as 0.5 nm along all directions. For the unit cell consisting of a single PA system, periodic boundary condition is used along  $x$ - and  $y$ -axes ( $xy$ -plane is where antenna system lies) to create the periodic array behavior and perfectly matched layer boundary condition is used along  $z$ -axis (propagation direction). The figure demonstrates the multiple absorption resonances (locating at 3 wavelengths,  $\lambda_1$ ,  $\lambda_2$  and  $\lambda_3$ ) supported by the U-bar shaped PA with  $L = 1200$  nm,  $H = 700$  nm,  $K = 1000$  nm,  $a = 50$  nm,  $b = 100$  nm,  $s = 100$  nm and array periodicity 1400 nm.

The working principle of our composite PA system relies on the interaction of magnetic and electric fields generated in different compartments of the PA. Basically, the top metal layer is patterned as subwavelength antennas serving as resonator while the bottom gold layer serves as an optical mirror, which significantly attenuates the transmittance. The incident light couples to nano-antennas resulting in an electric field. The nearfield couplings between the antennas and the

metal sheet result in mirror-image charges at the bottom metal layer, which induces a current loop. This current generates a magnetic field between the two metal layers. By selecting the optimum amplitude and the resonance frequency of the electric and magnetic fields, the PA impedance can be matched to free-space so that the reflectance can be minimized. At the same time, minimizing the reflectance with attenuating the transmission results in perfect absorption. The frequencies where we aimed to generate perfect absorption are chosen in such a way to overlap with vibrational fingerprints of the molecules for SEIRA applications. Fig. 2 shows the charge distributions of the PA platform, calculated by FDTD calculations. Here, surface currents of multi-band PA are investigated at resonating antenna elements and bottom ground plane for antenna modes at  $\lambda_1$ ,  $\lambda_2$  and  $\lambda_3$ , respectively. As shown in Fig. 2a–c, the electric field at  $\lambda_1$  is due to the opposite charges at top and bottom edges of the U-shape antenna, the one at  $\lambda_2$  is due opposite charges at nano-bar, and the one at  $\lambda_3$  is due to the opposite charges at the right and left edges of the U-shape antenna. The mirror-image charges in the gold plane (Au sheet in the figure), other words the charges opposite to the ones generated at the U-bar shaped antenna, interacts with then generates a current loop (illustrated with arrows), inducing a magnetic field (Fig. 2d–f).

## 2. Working mechanism of the multiband behavior

In order to understand the physical origin of the resonances supported by the PA system, we performed FDTD simulations of the PA system under an  $x$ -polarized light source. In the simulations, we used periodic boundary conditions along the  $x$  and  $y$ -axes and perfectly matched layer (PML) boundary condition along the  $z$ -axis. In Fig. 2, the field intensity distributions  $|E|^2$  at the top surface of the U-bar shape antennas were shown for the resonances at  $\lambda_1$ ,  $\lambda_2$  and  $\lambda_3$ . Here, the first and third modes are mainly concentrated at U-shape antenna and the second mode is concentrated at the nano-bar antenna.

Fig. 3 shows the dependence of the resonances supported by the PA system on different geometrical parameters, which enables a fine-tuning mechanism for optical responses matching vibrational modes of interest in SERIA applications. In our numerical analysis, the length of nano-bar ( $L$ ), the width ( $K$ ) and the height of the U-shape antenna, and the space between these constituent elements ( $s$ ) are tuned one at a time while others are kept constant. As it is shown in Fig. 3a, the increase in  $L$  shifts the mode at  $\lambda_1$  toward longer wavelengths, while the modes at  $\lambda_1$  and  $\lambda_3$  spectrally remain constant. As shown by the near-field calculations, as the local electromagnetic fields concentrate at the edges of the nano-bar, the variations in  $L$  significantly affect the spectral position of the mode at  $\lambda_1$ . The increase in  $H$  (Fig. 3b) and  $K$  (Fig. 3c) shifts the modes at  $\lambda_1$  and  $\lambda_3$  toward longer wavelengths due to the local electromagnetic field concentrated at U-shaped antennas. On the other hand, the modes at the mode  $\lambda_2$  do not show any spectral

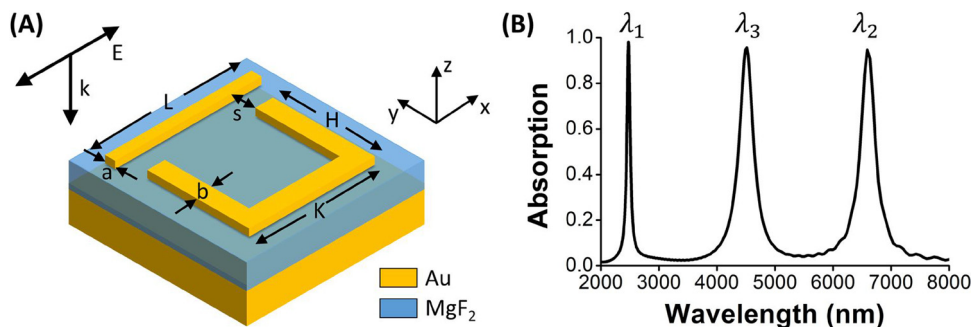
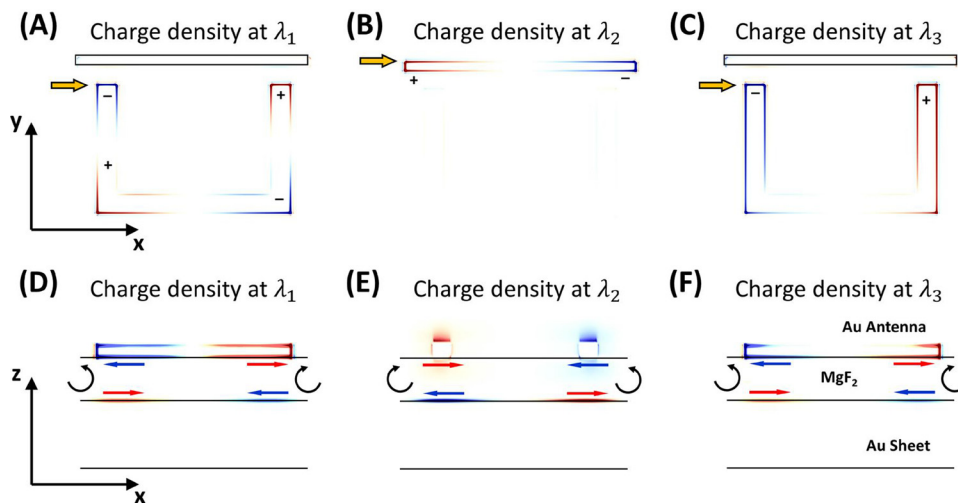


Fig. 1. (a) Schematic view of the U-bar shaped PA system. The geometrical device parameters are  $L$  (length of the nano-bar),  $H$  (height of the U-shape antenna),  $K$  (width of U-shape antenna),  $a$  (nano-bar width),  $s$  (distance between U-shape and nano-bar antennas),  $b$  (width of nano-bar in U-shape antenna). The U-bar antennas stand on a  $\text{SiO}_2$  layer on top of gold on top of Si substrate. In the figure, directions of polarization and propagation of the incident light source are shown. (b) Calculated multiple absorption response of the U-bar shaped PA with  $L = 1200$  nm,  $H = 700$  nm,  $K = 1000$  nm,  $a = 50$  nm,  $b = 100$  nm,  $s = 100$  nm and array periodicity 1400 nm. The thicknesses of the U-bar antennas,  $\text{SiO}_2$  layer and bottom gold plane are 40 nm, 140 and 200 nm, respectively.



**Fig. 2.** Charge density distributions (exhibiting a dipolar electric resonance) calculated (a–c) at the top surface of the antennas and (d–f) through cross-section for antenna modes at  $\lambda_1$ ,  $\lambda_2$  and  $\lambda_3$ , respectively. The dipolar electric charges induce electric fields and the current loop (illustrated with arrows) between metal layers induce magnetic fields. The geometrical parameters are  $L = 1200$  nm,  $H = 700$  nm,  $K = 1000$  nm,  $a = 50$  nm,  $b = 100$  nm,  $s = 100$  nm and array periodicity 1400 nm. The thicknesses of the U-bar antennas, SiO<sub>2</sub> layer and bottom gold plane are 40 nm, 140 and 200 nm, respectively.

variation. In order to study the interaction between individual constituent resonator elements, we changed the packing density parameter, which is the relative distance between U-shaped antenna and nano-bar two. As shown in Fig. 3e, variations in  $s$  do not effect the spectral position if resonances, which demonstrate that the multi-band behavior of the PA platform is due to the superposition of the optical responses of individual PA elements. Our results show that we can spectrally tune the resonances, while keeping their strong absorption capability (Fig. 4).

### 3. SEIRA capacity of the perfect absorber system

In order to show the SEIRA capability of our PA platform, we first theoretically investigated the vibrational signatures of a protein bilayer composed of protein A/G and protein IgG. Based on the experimentally obtained complex permittivity of the protein bilayer by the infrared reflection absorption spectroscopy, we used a Lorentz model where we fitted 3 oscillators to the experimental data as

$$\epsilon_{bilayer} = \epsilon_{\infty} + \sum_{i=1}^3 S_i / (\omega_{p_i}^2 - \omega^2 - j\omega\gamma_{p_i})$$

Here, the high frequency constant term,  $\epsilon_{\infty} = 2.1901$ , the oscillator resonance frequency,  $\omega_{p_1} = 3.12 \times 10^{14}$  (rad/sec),  $\omega_{p_2} = 2.90 \times 10^{14}$  (rad/sec),  $\omega_{p_3} = 2.73 \times 10^{14}$  (rad/sec) and the damping frequency,  $\gamma_{p_1} = 0.98 \times 10^{13}$  (rad/sec),  $\gamma_{p_2} = 1.02 \times 10^{13}$  (rad/sec),  $\gamma_{p_3} = 0.95 \times 10^{13}$  (rad/sec) and the oscillator strength,

$S_1 = 2.6 \times 10^{27}$  (rad/sec)<sup>2</sup>,  $S_2 = 1.8 \times 10^{27}$  (rad/sec)<sup>2</sup>,  $S_3 = 0.5961 \times 10^{27}$  (rad/sec)<sup>2</sup>. Fig. 5a and b show the real and imaginary parts of the permittivity of the protein bilayer. In Fig. 5b, red line denotes Amide I band at  $\sim 6025$  nm corresponding to C=O stretching vibration, green line denotes Amide II at  $\sim 6562$  nm corresponding to C–N–H bending and C–N stretching vibrations and blue line denotes weak Amide III at  $\sim 6905$  nm. In our FDTD simulations, we used a protein bilayer with a thickness of  $\sim 8$  nm, which has been experimentally characterized through ellipsometry measurements (Woollam). We determined the protein vibrational signatures through monitoring the spectral changes in the reflection response of the PA. Fig. 5c–e shows the reflection response of the PA system for different H values e.g., 500, 600 and 700 nm, respectively to excite the mode at  $\lambda_3$  overlapping with Amide I, II and III vibration modes of the protein bilayer. Here, the vibrational signatures are observed as spectral dips in the reflection response due to the Amide modes, which absorbs light at this specific wavelength.

We also performed FDTD simulations to determine C=O band of PMMA. Fig. 6a and b show the real and imaginary part of PMMA permittivity determined by fitting a single Lorentz model as described previously,  $\epsilon_{bilayer} = \epsilon_{\infty} + (S / (\omega_p^2 - \omega^2 - i\omega\gamma_p))$ , where  $\epsilon_{\infty} = 2.36$ ,  $\omega_p = 3.26 \times 10^{14}$  (rad/sec),  $\gamma_p = 3.72 \times 10^{12}$  (rad/sec), and  $S = 1.22 \times 10^{27}$  (rad/sec)<sup>2</sup>. Fig. 6c shows the reflection spectra of the PA platform covered with PMMA, where the C=O band stretch (purple line) can be seen as a strong reflection dip.

As a first step to experimental demonstration of the SEIRA capacity

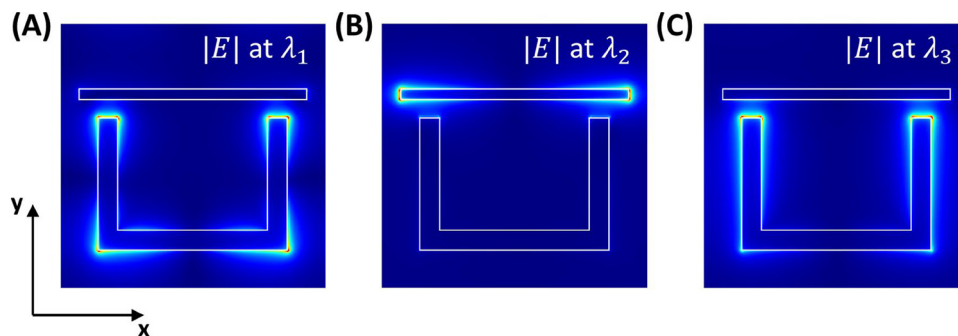


**Fig. 3.** Electric field intensity distributions ( $|E|^2$ ) of the U-bar shaped antenna structure at the top metal surface for the resonant modes at (a)  $\lambda_1$ , (b)  $\lambda_2$  and (c)  $\lambda_3$ , of the structure with the corresponding parameters. The geometrical parameters are  $L = 1200$  nm,  $H = 700$  nm,  $K = 1000$  nm,  $a = 50$  nm,  $b = 100$  nm,  $s = 100$  nm and array periodicity 1400 nm. The thicknesses of the U-bar antennas, SiO<sub>2</sub> layer and bottom gold plane are 40 nm, 140 and 200 nm, respectively.

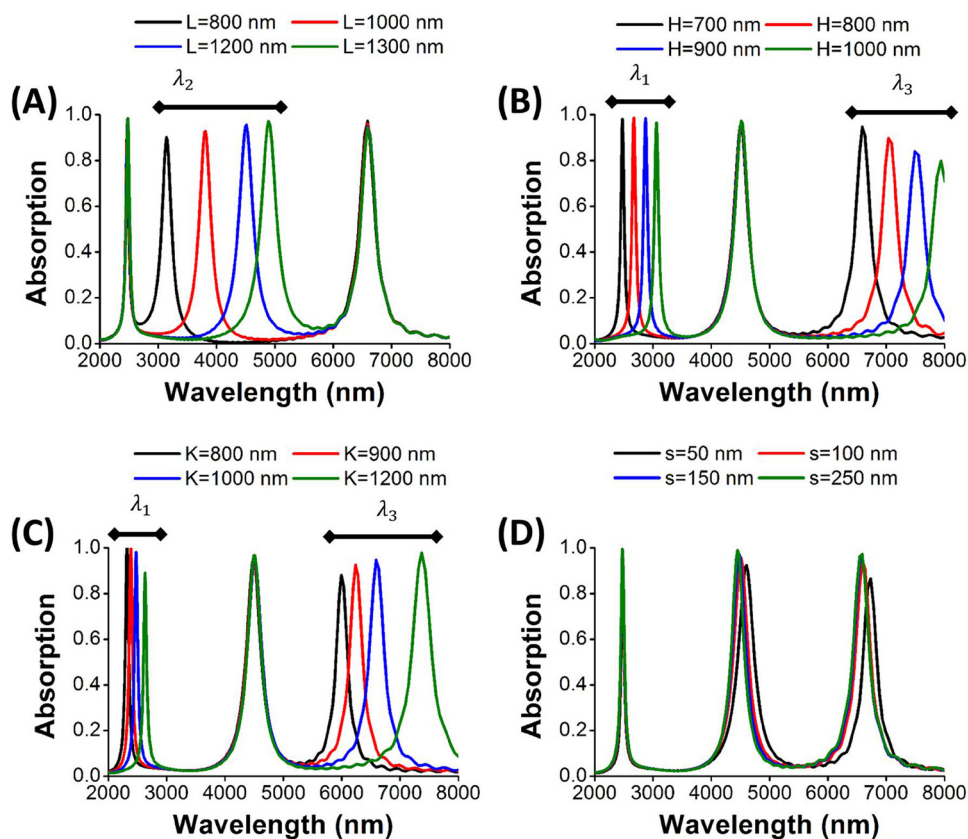


Fig. 4. Calculated absorption spectra of U-bar shaped antenna arrays. (a) with  $L = 800$  nm,  $1000$  nm,  $1200$  nm,  $1300$  nm, where  $K = 1000$  nm,  $H = 700$  nm,  $a = 50$  nm,  $b = 100$  nm,  $s = 100$  nm and array periodicity  $1400$  nm. (b) with  $H = 700$  nm,  $800$  nm,  $900$  nm,  $1000$  nm, where  $K = 1000$  nm,  $L = 1200$  nm,  $a = 50$  nm,  $b = 100$  nm,  $s = 100$  nm and array periodicity  $1400$  nm. (c) with  $K = 800$  nm,  $900$  nm,  $1000$  nm, where  $L = 1200$  nm,  $H = 700$  nm,  $a = 50$  nm,  $b = 100$  nm,  $s = 100$  nm and array periodicity  $1400$  nm. (d) with  $s = 50$  nm,  $100$  nm,  $150$  nm,  $250$  nm, where  $K = 1000$  nm,  $L = 1200$  nm,  $H = 700$  nm,  $a = 50$  nm,  $b = 100$  nm and array periodicity  $1400$  nm.

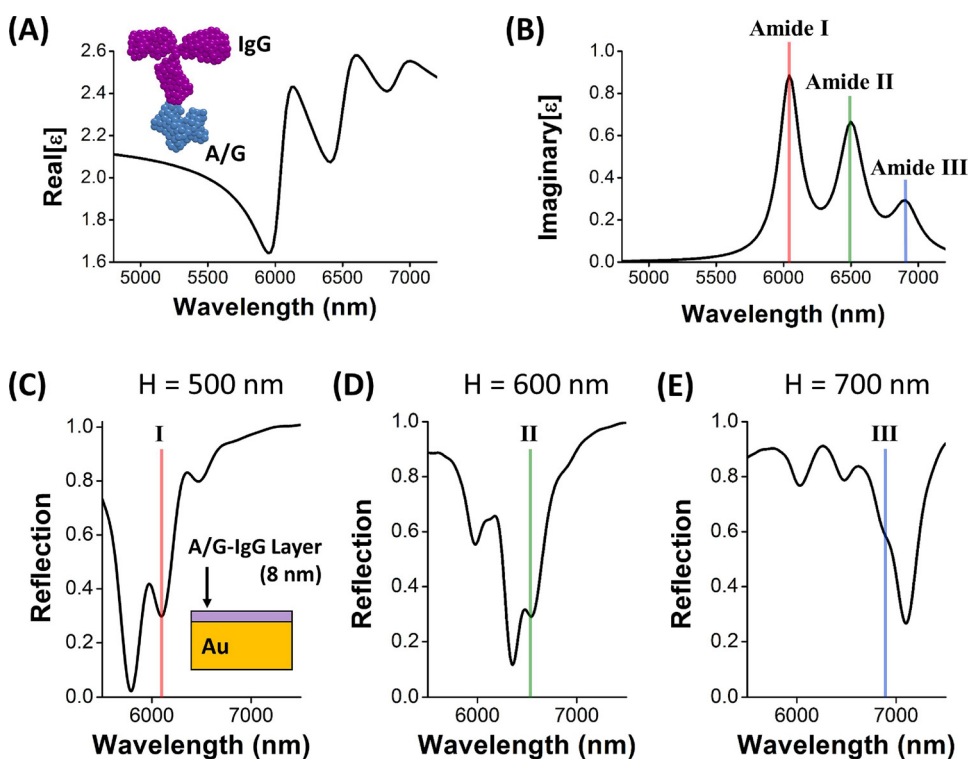
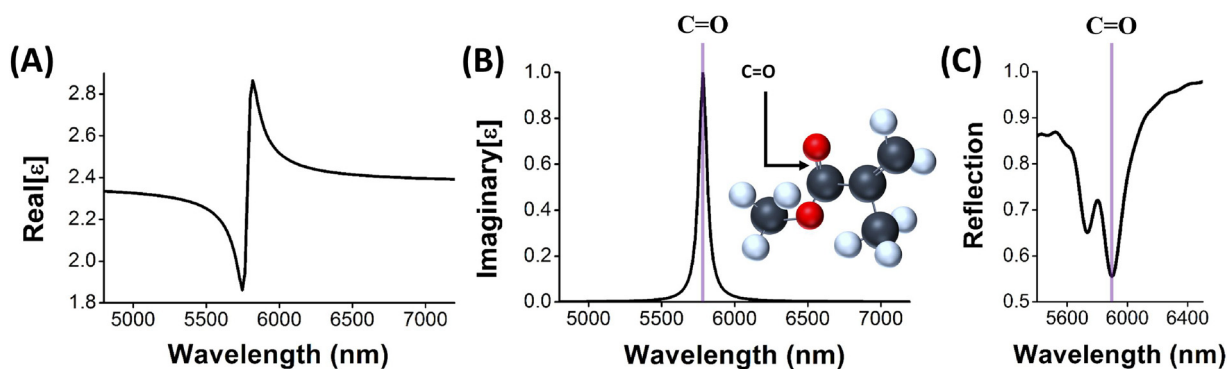


Fig. 5. (a) Real and (b) imaginary parts of the modeled permittivity function for the protein bilayer consisting of proteins A/G and IgG. Calculated reflection response of the PA platform covered with  $8$  nm, where  $H$  is modified ( $500$ ,  $600$  and  $700$  nm) to match with (c) Amide I (red line), (d) Amide II (green line), and (e) Amide III (blue line) bands of the protein bilayer. The geometrical parameters are  $L = 1200$  nm,  $K = 1000$  nm,  $a = 50$  nm,  $b = 100$  nm,  $s = 100$  nm and array periodicity  $1400$  nm. The thicknesses of the U-bar antennas,  $\text{SiO}_2$  layer and bottom gold plane are  $40$  nm,  $140$  and  $200$  nm, respectively. (For interpretation of the references to colour in this figure legend, the reader is referred to the web version of this article).

of our perfect absorber platform, we fabricated the PA platform to measure the C=O vibrational band of PMMA. The fabrication of PA consists of metal deposition, electron beam lithography (EBL) and lift-off process. All arrays are fabricated as  $100 \times 100 \mu\text{m}^2$  squares on one single Si wafer chip. Initially, Si wafer was cleaned with standard

cleaning procedure. Then,  $5$  nm of Ti and  $200$  nm of Au, and  $140$  nm of  $\text{SiO}_2$  are deposited onto the Si substrate by using electron beam evaporator (Angstrom). Metals are with Kurt J. Lesker, 99.999% purity. For EBL process, a resist layer of PMMA (950 PMMA A3, MicroChem) was spin-coated over the  $\text{SiO}_2$  layer. After this step, EBL was performed with



**Fig. 6.** (a) Real and (b) imaginary parts of the PMMA permittivity. Figure inset shows the schematic illustration of protein vibrational modes. (c) Calculated reflectance spectrum of the PA coated with a 10 nm-thick PMMA layer. The geometrical parameters are  $L = 1200$  nm,  $H = 700$  nm,  $K = 1000$  nm,  $a = 50$  nm,  $b = 100$  nm,  $s = 100$  nm and array periodicity 1400 nm. The thicknesses of the U-bar antennas, SiO<sub>2</sub> layer and bottom gold plane are 40 nm, 140 and 200 nm, respectively. Purple line denotes C=O vibrational band of PMMA. (For interpretation of the references to colour in this figure legend, the reader is referred to the web version of this article).

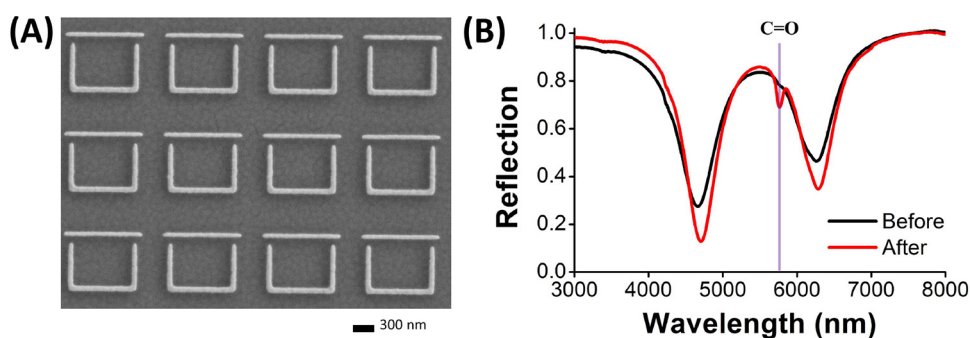


**Fig. 7.** (a) SEM image of the fabricated PA platform. (b) Measured reflectance spectra of a thick PMMA film covered on U-bar shaped PA platform. Black and red lines denoted the reflectance before and after the addition of the PMMA film. Purple line denotes C=O vibrational band of PMMA. The geometrical parameters are  $L = 1200$  nm,  $H = 700$  nm,  $K = 1000$  nm,  $a = 50$  nm,  $b = 100$  nm,  $s = 100$  nm and array periodicity 1400 nm. The thicknesses of the U-bar antennas, SiO<sub>2</sub> layer and bottom gold plane are 40 nm, 140 and 200 nm, respectively. (For interpretation of the references to colour in this figure legend, the reader is referred to the web version of this article).

is referred to the web version of this article).

Zeiss SUPRA 40 VP electron microscope. The patterned chips were developed in a methyl isobutyl ketone (MIBK)-isopropanol (IPA) solution (MIBK:IPA = 1:3). Later, 40 nm Au was deposited onto the developed substrate with 5 nm Ti for adhesion. Following that, the remaining resist layer was lifted off with acetone and IPA leaving the patterned arrays of U-bar shaped PA on the substrate. Finally, oxygen plasma clean with PVA TePla America M4 plasma asher was used to remove any remaining residues on the surface. The scanning electron microscope (SEM) image of the fabricated PA platform is shown in Fig. 7a. Fig. 7b shows the experimental result of the system covered with 10 nm PMMA (thickness of the PMMA film was calibrated with ellipsometry). The dip at  $1780\text{ cm}^{-1}$ , corresponds to C=O vibrational band of PMMA film. The spectral data taken with Bruker Vertex Fourier transform infrared spectrometer that is coupled to a Hyperion 1000 IR microscope with a mirror velocity of 20 kHz and 256 scans. The spectral contribution of the antennas was normalized to background signal, obtained from a reference gold mirror in order to eliminate any background signal.

#### 4. Conclusions

In this work, we introduced a platform based on multi-band perfect absorber for SEIRA applications to detect multiple fingerprints of bio-and chemical molecules. We showed the working principle of the near-unity absorption at multiple spectral points and the physical origin of the multiple antenna modes supported by the PA system. We investigated a fine-tuning mechanism of multiple absorption resonances through geometrical parameters. We theoretically showed the SEIRA capability of our system by monitoring the absorption signals of protein bilayers and polymer films coating the surface of the PA platform. We theoretically showed the SEIRA capability of our system by monitoring the

absorption signals of protein bilayers and polymer films based on PA platform. Our platform is very promising for simultaneous detection of multiple vibrational modes of the same molecules, which could provide more reliable sensing information over the system relying only on a single vibrational mode.

#### Acknowledgements

Habibe Durmaz acknowledges the support of Recep Tayyip Erdogan University Scientific Research Foundation (project No: FUA-2017-762) and Boston University Photonics Center.

#### References

- [1] V.M. Shalaev, Optical negative-index metamaterials, *Nat. Photonics* 1 (2007) 41–48, <https://doi.org/10.1038/nphoton.2006.49>.
- [2] R. Fleury, D.L. Sounas, A. Alù, Negative refraction and planar focusing based on parity-time symmetric metasurfaces, *Phys. Rev. Lett.* 113 (2014) 023903, <https://doi.org/10.1103/PhysRevLett.113.023903>.
- [3] A.C. Atre, A. García-Etxarri, H. Alaeian, J.A. Dionne, A broadband negative index metamaterial at optical frequencies, *Adv. Opt. Mater.* 1 (2013) 327–333, <https://doi.org/10.1002/adom.201200022>.
- [4] H.X. Xu, G.M. Wang, M.Q. Qi, L. Li, T.J. Cui, Three-dimensional super lens composed of fractal left-handed materials, *Adv. Opt. Mater.* 1 (2013) 495–502, <https://doi.org/10.1002/adom.201300023>.
- [5] O.V. Minin, I.V. Minin, Terahertz artificial dielectric cuboid lens on substrate for super-resolution images, *Opt. Quantum Electron.* 49 (2017) 326–329, <https://doi.org/10.1007/s11082-017-1165-6>.
- [6] J. Valentine, J. Li, T. Zentgraf, G. Bartal, X. Zhang, An optical cloak made of dielectrics, *Nat. Mater.* 8 (2009) 568–571, <https://doi.org/10.1038/nmat2461>.
- [7] T. Ergin, N. Stenger, P. Brenner, J.B. Pendry, M. Wegener, Three-dimensional invisibility cloak at optical wavelengths, *Science* 328 (2010) 337–339, <https://doi.org/10.1126/science.1186351>.
- [8] X. Ni, Z.J. Wong, M. Mrejen, Y. Wang, X. Zhang, An ultrathin invisibility skin cloak for visible light, *Science* 349 (2015) 1310–1314, <https://doi.org/10.1126/science.aac9411>.
- [9] K. Aydin, V.E. Ferry, R.M. Briggs, H.A. Atwater, Broadband polarization-

- independent resonant light absorption using ultrathin plasmonic super absorbers, *Nat. Commun.* 2 (2011) 517, <https://doi.org/10.1038/ncomms1528>.
- [10] J. Rosenberg, R.V. Sheno, T.E. Vandervelde, S. Krishna, Q. Painter, A multi-spectral and polarization-selective surface-plasmon resonant mid-infrared detector, *Appl. Phys. Lett.* 95 (2009) 161101–161103, <https://doi.org/10.1063/1.3244204>.
- [11] W.L. Huang, H.H. Hsiao, M.R. Tang, S.C. Lee, Triple-wavelength infrared plasmonic thermal emitter using hybrid dielectric materials in periodic arrangement, *Appl. Phys. Lett.* 109 (2016) 063107, <https://doi.org/10.1063/1.4960664>.
- [12] Z. Zhang, J. Yang, X. He, J. Zhang, J. Huang, D. Chen, Y. Han, Plasmonic refractive index sensor with high figure of merit based on concentric-rings resonator, *Sensors* 18 (2018) 116, <https://doi.org/10.1364/OE.22.025931>.
- [13] B. Yun, G. Hu, Y. Cui, Theoretical analysis of a nanoscale plasmonic filter based on a rectangular metal–insulator–metal waveguide, *J. Phys. D Appl. Phys.* 43 (2010) 385102, <https://doi.org/10.1088/0022-3727/43/38/385102>.
- [14] Q. Yang, J. Gu, D. Wang, X. Zhang, Z. Tian, C. Ouyang, R. Singh, J. Han, W. Zhang, Efficient flat metasurface lens for terahertz imaging, *Opt. Express* 22 (2014) 25931–25939, <https://doi.org/10.1364/OE.22.025931>.
- [15] A.W. Lee, Q. Hu, Real-time, continuous-wave terahertz imaging by use of a microbolometer focal-plane array, *Opt. Lett.* 30 (2005) 2563–2565, <https://doi.org/10.1364/OL.30.002563>.
- [16] N.I. Landy, S. Sajuyigbe, J.J. Mock, D.R. Smith, W.J. Padilla, Perfect metamaterial absorber, *Phys. Rev. Lett.* 100 (2008) 207402, <https://doi.org/10.1103/PhysRevLett.100.207402>.
- [17] N. Liu, M. Mesch, T. Weiss, M. Hentschel, H. Giessen, Infrared absorber and its applications as plasmonic sensor, *Nano Lett.* 10 (2010) 2342–2348, <https://doi.org/10.1021/nl904103>.
- [18] A.E. Cetin, S. Korkmaz, H. Durmaz, E. Aslan, E. Aslan, S. Kaya, R. Paiella, M. Turkmen, Quantification of multiple molecular fingerprints by dual-resonant perfect absorber, *Adv. Opt. Mater.* 4 (2016) 1274–1280, <https://doi.org/10.1002/adom.201600305>.
- [19] T. Xie, Z. Chen, R. Ma, M. Zhong, A wide angle and polarization insensitive infrared broadband meta-material absorber, *Opt. Commun.* 383 (2017) 81–86, <https://doi.org/10.1016/j.optcom.2016.08.058>.
- [20] B. Mulla, C. Sabah, Multiband metamaterial absorber design based on plasmonic resonances for solar energy harvesting, *Plasmonics* 11 (2016) 1313–1321, <https://doi.org/10.1007/s11468-015-0177>.
- [21] Y. Avitzour, Y.A. Urzhumov, G. Shvets, Wide-angle infrared absorber based on negative index plasmonic metamaterial, *Phys. Rev. B* 79 (2009) 045131–045136, <https://doi.org/10.1103/PhysRevB.79.045131>.
- [22] N.I. Landy, S. Sajuyigbe, J.J. Mock, D.R. Smith, W.J. Padilla, Perfect meta-material absorber, *Phys. Rev. Lett.* 100 (2008) 207402–207405, <https://doi.org/10.1103/PhysRevLett.100.207402>.
- [23] C.W. Cheng, M.N. Abbas, C.W. Chiu, K.T. Lai, M.H. Shih, Y.C. Chang, Wide-angle polarization independent infrared broad band absorbers based on metallic multi sized disk arrays, *Opt. Express* 20 (2012) 10376–10381, <https://doi.org/10.1364/OE.20.010376>.
- [24] H. Cheng, S.Q. Chen, H.F. Yang, J.J. Li, X. An, C.Z. Gu, J.G. Tian, A polarization insensitive and wide-angle dual-band nearly perfect absorber in the infrared regime, *J. Opt.* 14 (2012) 085102–085106, <https://doi.org/10.1088/2040-8978/14/8/085102>.
- [25] Z.J. Zhang, R.W. Peng, Z. Wang, F. Gao, X.R. Huang, W.H. Sun, Q.J. Wang, M. Wang, Plasmonic antenna array at optical frequency made by nanoapertures, *Appl. Phys. Lett.* 93 (2008) 171110, <https://doi.org/10.1063/1.3010741>.
- [26] G. Kumar, S. Li, M.M. Jadidi, T.E. Murphy, Terahertz surface plasmon waveguide based on a one-dimensional array of silicon pillars, *New J. Phys.* 15 (2013) 085031, <https://doi.org/10.1088/1367-2630/15/8/085031>.
- [27] K. Chen, R. Adato, H. Altug, Dual-band perfect absorber for multispectral plasmon-enhanced infrared spectroscopy, *ACS Nano* 6 (2012) 7998–8006, <https://doi.org/10.1021/nn3026468>.
- [28] J. Kundu, F. Le, P. Nordlander, N.J. Halas, Surface enhanced infrared absorption (SEIRA) spectroscopy on nanoshell aggregate substrates, *Chem. Phys. Lett.* 452 (2008) 115–119, <https://doi.org/10.1016/j.cplett.2007.12.042>.
- [29] Y. Li, L. Su, C. Shou, C. Yu, J. Deng, Y. Fang, Surface-enhanced molecular spectroscopy (SEMS) based on perfect-absorber metamaterials in the mid-infrared, *Sci. Rep.* 3 (2013) 2865, <https://doi.org/10.1038/srep02865>.
- [30] B. Cerjan, X. Yang, P. Nordlander, N.J. Halas, Asymmetric aluminum antennas for self-calibrating surface-enhanced infrared absorption spectroscopy, *ACS Photonics* 3 (2016) 354–360, <https://doi.org/10.1021/acsp Photonics.6b00024>.
- [31] C.K. Chen, M.H. Chang, H.T. Wu, Y.C. Lee, T.J. Yen, enhanced vibrational spectroscopy, intracellular refractive indexing for label-free biosensing and bioimaging by multiband plasmonic- antenna array, *Biosens. Bioelectron.* 60 (2014) 343–350, <https://doi.org/10.1016/j.bios.2014.04.019>.
- [32] H. Tang, G. Meng, Z. Li, C. Zhu, Z. Huang, Z. Wang, F. Li, Hexagonally arranged arrays of urchin-like Ag hemispheres decorated with Ag nanoparticles for surface-enhanced Raman scattering substrates, *Nano Res.* 8 (2015) 2261–2270, <https://doi.org/10.1007/s12274-015-0737-7>.
- [33] X. Zhang, Y. Zheng, X. Liu, L. Wei, J. Dai, D.Y. Lei, D.R. MacFarlane, Hierarchical porous plasmonic metamaterials for reproducible ultrasensitive surface-enhanced Raman spectroscopy, *Adv. Mater.* 27 (2015) 1090–1096, <https://doi.org/10.1002/adma.201404107>.
- [34] M. Zheng, X. Zhu, Y. Chen, Q. Xiang, H. Duan, Three-dimensional donut-like gold nanorings with multiple hot spots for surface-enhanced Raman spectroscopy, *Nanotechnology* 28 (2017) 45303, <https://doi.org/10.1088/1361-6528/28/4/045303>.
- [35] Ferdows B. Zarrabi, Sub-wavelength plasmonic nano-antenna with H and U shape for enhancement of multi resonance, *Optik* (2016), <https://doi.org/10.1016/j.jl.2016.01.189>.

**Habibe Durmaz** is an Assistant Professor in the Department of Electrical and Electronics Engineering at Recep Tayyip Erdogan University, Rize, Turkey. Dr. Durmaz received her B.S. degree from Selcuk University, Konya, Turkey and M.S. degree from Temple University, Philadelphia, PA, USA both in Physics. She received her Ph.D. degree in Electrical Engineering from Boston University, Boston, MA, USA in 2016. She worked as a visiting faculty at Boston University between April 2017 and July 2017. Dr. Durmaz's current research interests include optoelectronic materials and devices, quantum photodetectors and lasers, graphene plasmonics, bio- and chemical detection, metamaterials, and nanophotonics.

**Yuyu Li** received his MS degree in Physics from Boston University, Massachusetts, USA. He is currently pursuing Electrical Engineer PhD in the same University. Li received his BS degree in Theoretic Physics from Shandong University, Shandong, China and MS degree in Applied Physics from Umass Boston, Massachusetts, USA. Li's bachelor thesis was on ultrafast laser and nonlinear optics applications. Later during his master in Umass, he focused on biophotonics. To study vivid topological growing of tumor, he combined digital holography microscopy with confocal microscopy, the results are coincident with the tumor volume growing trend in theory. He also developed a new Fourier microscopy technique by using multi-wavelength. Currently, Li focuses on Terahertz emitters and detectors using quantum structures and 2D materials. Li also studies metasurface applications.

**Arif E. Cetin** is a Research Group Leader in Izmir Biomedicine and Genome Center (IBG), locating in Izmir, Turkey. Dr. Cetin received his BS degree in Electrical and Electronics Engineering and MS degree in Electrical and Computer Engineering both from Koc University, Istanbul, Turkey. He received his PhD degree in Electrical Engineering from Boston University, Boston, MA, USA. He worked as a postdoctoral associate at EPFL (Swiss Federal School in Lausanne), Switzerland in 2013–2014, as a postdoctoral fellow at Massachusetts Institute of Technology, Cambridge, MA, USA in 2014–2016 and as a research scientist at Omniome, San Diego, CA, USA in 2016–2018. Dr. Cetin pursued research on optical nano-biosensors integrated with microfluidic platforms for ultra-sensitive label-free biodetection. He developed hand-held biosensors for high-throughput and multiplexed biosensing for resource-poor settings. Dr. Cetin developed electro-mechanical sensors for growth rate cytometer to determine therapeutic susceptibility of cancer cells for personalized drug therapy. Recently, he also developed a unique label-free technique for high-throughput DNA sequencing. Dr. Cetin is the author of 30 articles and contributor of more than 50 scientific talks.